

Nanoscale

Accepted Manuscript



This is an *Accepted Manuscript*, which has been through the Royal Society of Chemistry peer review process and has been accepted for publication.

Accepted Manuscripts are published online shortly after acceptance, before technical editing, formatting and proof reading. Using this free service, authors can make their results available to the community, in citable form, before we publish the edited article. We will replace this *Accepted Manuscript* with the edited and formatted *Advance Article* as soon as it is available.

You can find more information about *Accepted Manuscripts* in the [Information for Authors](#).

Please note that technical editing may introduce minor changes to the text and/or graphics, which may alter content. The journal's standard [Terms & Conditions](#) and the [Ethical guidelines](#) still apply. In no event shall the Royal Society of Chemistry be held responsible for any errors or omissions in this *Accepted Manuscript* or any consequences arising from the use of any information it contains.



Journal Name

ARTICLE

Adsorption of Doxorubicin on Citrate-Capped Gold Nanoparticles: Insights into Engineering Potent Chemotherapeutic Delivery Systems

Received 00th January 20xx,
Accepted 00th January 20xx

DOI: 10.1039/x0xx00000x

www.rsc.org/

Dennis Curry^{a,c}, Amanda Cameron^a, Bruce MacDonald^b, Collins Nganou^a, Hope Scheller^{a,f}, James Marsh^b, Stefanie Beale^d, Mingsheng Lu^a, Zhi Shan^a, Rajandra Kaliaperumal^{al}, Heping Xu^e, Mark Servos^c, Craig Bennett^d, Stephanie MacQuarrie^b, Ken D. Oakes^{a,f}, Martin Mkandawire^a, and Xu Zhang^{a*}

Gold nanomaterials have received great interest for their use in cancer theranostic applications over the past two decades. Many gold nanoparticle-based drug delivery system designs rely on adsorbed ligands such as DNA or cleavable linkers to load therapeutic cargo. The heightened research interest was recently demonstrated in the simple design of nanoparticle-drug conjugates wherein drug molecules are directly adsorbed onto the as-synthesized nanoparticle surface. The potent chemotherapeutic, doxorubicin often serves as a model drug for gold nanoparticle-based delivery platforms; however, the specific interaction facilitating adsorption in this system remains understudied. Here, for the first time, we propose empirical and theoretical evidence suggestive of the main adsorption process where 1) hydrophobic forces drive doxorubicin towards the gold nanoparticle surface before 2) cation- π interactions and gold-carbonyl coordination between the drug molecule and the cations on AuNP surface facilitate DOX adsorption. In addition, biologically relevant compounds, such as serum albumin and glutathione, were shown to enhance desorption of loaded drug molecules from AuNP at physiologically relevant concentrations, providing insight into the drug release and *in vivo* stability of such drug conjugates.

Introduction

Doxorubicin (DOX), an anthracycline chemotherapeutic, remains at the forefront of malignant breast, leukemic and sarcoma cancer treatment more than 30 years after its clinical inception and FDA approval.¹ Despite its widespread usage, DOX is often associated with multidrug resistance (MDR) as well as adverse side effects such as nausea, hair loss and acute and chronic cardiotoxicity, the latter potentially leading to congestive heart failure.^{2,3,4,5} Liposomal formulations of DOX have led to

improvements in the drug's efficiency but the development of advanced targeted drug delivery system (DDS) platforms for DOX remains a worthwhile research endeavour receiving substantial investment.^{6,7,8,9,10} An ideal targeted DOX delivery platform would decrease required concentrations as well as the prevalence and intensity of side effects associated with the drug, all while utilizing its potent anti-cancer properties.¹¹

Gold nanoparticles (AuNPs) have become an increasingly popular DDS development in recent years.^{12,13,14,15,16} High biocompatibility, tunable surface chemistry and unique optical properties make nanogold a desirable platform for many biomedical applications.^{17,18,19,20} Further, AuNPs have been commercialized for use in diagnostic applications and are involved in clinical-phase trials.^{21,22,23} Numerous studies have highlighted AuNPs promise in the targeted delivery of anticancer drugs including DOX to cancerous cells and tissue.^{14, 24} Gold nanorods (AuNRs) and hollow gold nanoparticles (HGNs) allowing for the absorption of tissue-penetrating near-infrared (NIR) light have been successfully used in combinational chemophotothermal therapy (PTT) and imaging applications.^{25,26,27,28}

¹Current address: Department of Biotechnology, Periyar Maniammai University, Vallam, Thanjavur, Tamil Nadu, India.

²Verschuren Centre for Sustainability in Energy and the Environment, Cape Breton University, 1250 Grand Lake Rd, Sydney, Nova Scotia, B1P 6L2, Canada.
Email: Xu_Zhang@CBU.ca

³Department of Chemistry, Cape Breton University, 1250 Grand Lake Rd, Sydney, Nova Scotia, B1P 6L2, Canada

⁴Department of Biology, University of Waterloo, Waterloo, Ontario, N2L 3G1, Canada

⁵Department of Physics, Acadia University, Wolfville, Nova Scotia, B4P 2R6, Canada

⁶Cape Breton Cancer Centre, Cape Breton Regional Hospital, Sydney, Nova Scotia, B1P 1P3, Canada

⁷Department of Biology, Cape Breton University, 1250 Grand Lake Rd, Sydney, Nova Scotia, B1P 6L2, Canada

Electronic Supplementary Information (ESI) available: [details of any supplementary information available should be included here]. See DOI: 10.1039/x0xx00000x

Currently, there are two mechanisms for loading DOX to nanogold delivery vehicles. The first approach is through indirect attachment with thiolated anchor molecules such as methoxy-poly ethylene glycol (mPEG),²⁹ double-stranded DNA rich with G-C base-pairs⁹, and copolymers.³⁰ In this system, controlled release of DOX can be efficiently achieved via either temperature induced DNA melting or pH-sensitive cleavage (i.e., acid-cleavable hydrazone linkage).²⁴ The second approach is the direct adsorption of DOX onto gold surfaces.^{27,31,32} DOX has been demonstrated to have high affinity for various gold nanomaterials such as solid AuNPs, AuNRs and HGNS. HGNS showed exceptionally high loading of DOX due to their high surface area.²⁷ In contrast to the elegant, controllable, yet complicated indirect DOX loading procedure, direct adsorption is simple and straightforward, but the physicochemical interaction mechanism between DOX and AuNPs remains largely understudied, with only limited reports discussing potential interaction mechanisms available at present. In these reports, an electrostatic interaction between the positively-charged amine moiety of DOX and the negatively-charged citrate that serves as the capping ligand on the surface of AuNPs is proposed to facilitate DOX adsorption,^{31,32} but, to date, such salt-bridging interactions have not been substantiated by systematic experimentation. The immense interest in AuNP-DOX based DDS development, together with limited mechanistic understanding of the system, motivated us to conduct more rigorous investigations better defining the physicochemical interactions driving DOX adsorption onto AuNP surfaces.

Results and discussion

Adsorption of DOX on AuNPs

The adsorption of DOX on AuNP surfaces was studied by fluorescence measurement, where AuNPs serve as an excellent quencher of the fluorescence signal of DOX upon adsorption via nanoparticle surface energy transfer (NSET). Isotherm data in Figure 1A depicts a Langmuir adsorption behavior with maximum DOX loading of ~550 drug molecules per AuNP (citrate capped, ~13 nm in diameter), indicating monolayer adsorption of DOX on the AuNP surface.³³ The adsorption process was complete in less than 30 seconds (Figure 1B), suggestive of diffusion-limited kinetics. Meanwhile, DOX adsorption was accompanied by an aggregation of AuNPs, characterized by color change of the AuNP solution from wine red to purple, as shown in the red-shifted absorbance spectra (Figure S1) and TEM images of DOX-AuNP conjugates (Figures

S2-4). One explanation may be that when DOX adsorbs onto the

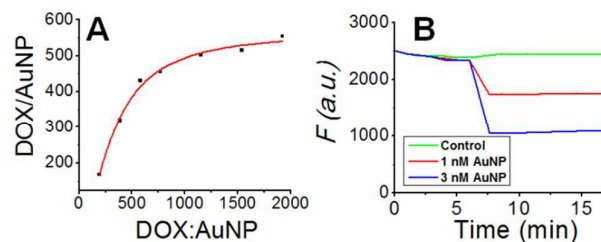
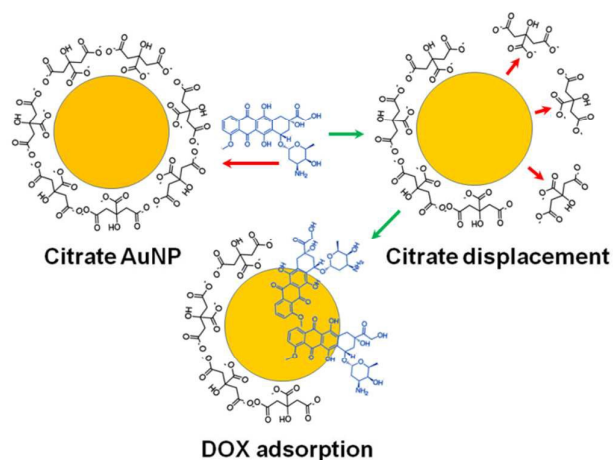


Figure 1. (A) DOX-AuNP isotherm including Langmuir Fit (solid line). DOX added = DOX:AuNP molar concentration ratio. See Figure S7A for original data with standard errors. (B) DOX fluorescence decrease upon addition of AuNP.

surface of the AuNPs, the negatively charged citrate anions, originally adsorbed on AuNP surfaces and providing electrostatic stabilization, are replaced by DOX. Such replacement may destabilize AuNPs in solution by decreasing repulsive forces, resulting in AuNP aggregation due to gold's high density and strong van der Waals forces between particles in solution³⁴. Another mechanism may be due to salt-bridging of the negatively charged citrate-coated AuNPs by DOX via its amine group, which is positively charged under neutral pH regimes. To verify these hypotheses, we monitored the displacement of citrate from AuNP surface by DOX using fluorescence spectroscopy. The results indicated that ~505 citrate ions were replaced by DOX molecules from each AuNP surface (Figure S5). Considering the size and charge of citrate and the surface area of each AuNP, most of the adsorbed citrate molecules were replaced by DOX molecules. Despite the persistent existence of citrate on the surface of AuNPs, as pointed out by J. Park *et al.*³⁵, essentially most DOX molecules were adsorbed directly on AuNP surfaces, discrediting the salt-bridge mechanism.

The replacement of citrate by DOX (Scheme 1) was further supported by the results obtained with Fourier Transform Infrared Spectroscopy (FTIR). Spectral analysis of the DOX-AuNP conjugates and citrate-AuNP reveals the existence of much more free citrate (a pronounced peak at 1394 cm^{-1}) in the DOX-AuNP samples than in the citrate-AuNP sample (Figure S6).³⁶ In addition, the adsorption of DOX on AuNP surfaces was distinctive, as evidenced by a larger peak at 1589 cm^{-1} , assigned to the C=O bond at the 13-keto position of DOX.³⁷



Scheme 1. Citrate displacement from AuNP surface upon addition of DOX.

A further question is to identify the driving force underlying DOX adsorption. We assume that electrostatic attraction (between the citrate anions on AuNPs and the positively charged amine group in DOX) may drive the DOX to approach AuNP surfaces, thus facilitating their adsorption even though the DOX-AuNP interaction itself was not based on a salt-bridging mechanism.^{33,38,39} To evaluate this hypothesis, we studied the effect of NaCl concentrations and solution pH on DOX adsorption. When adding DOX solution spiked with various NaCl concentrations into the AuNP solution (volume ratio 1:1 which is critical to ensure fast mixing and even DOX adsorption onto each AuNP), the results indicated no decrease in DOX adsorption capacity even with 136 mM NaCl in the solution (Figure 2A), suggesting high Na^+ concentrations did not interfere with DOX adsorption, confirming adsorption was not driven by electrostatic attraction.⁴⁰ As shown in Figure 2B, similar results were observed with pH influences. Lower pH values (e.g., pH 3) promote complete protonation of DOX, decreasing DOX adsorption slightly (< 10%), while providing further evidence against the salt-bridging electrostatic mechanism. These findings were further confirmed with the results of desorption experiments, where the increase in DOX fluorescence signal due to dissociation of DOX-AuNP conjugates was monitored under various pH conditions. Herein, low pH environments facilitated more desorption (~10%) than alkaline environments (Figure 3A). Since adjusting pH is an effective means to alter the charge states of the species involved, again, our results disfavor the electrostatic attraction based adsorption theory. Instead, the pH effect could be explained if DOX adsorption was driven by hydrophobic forces, where at lower pH, DOX molecules were completely ionized and displayed less hydrophobicity, resulting in lower adsorption and higher desorption, similar to the effect of pH on DOX adsorption onto carbon nanotubes.⁴¹

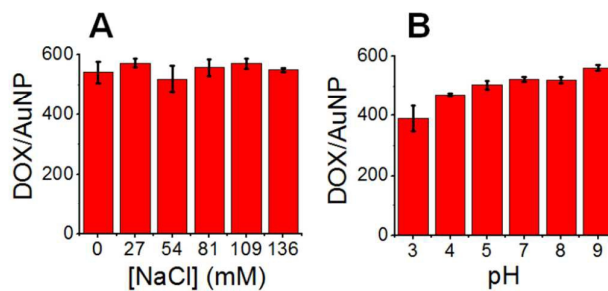


Figure 2. Adsorption of DOX onto AuNP in presence of varying NaCl concentrations (A) and pH environments (B).

As shown in Figure 3B, when using solvents with decreasing polarity (pure water, 33% methanol, and ethanol aqueous solutions), more DOX molecules were desorbed from AuNP surfaces to the solvent, suggesting DOX hydrophobic functional groups are involved in the interaction with AuNPs, consistent with the pH effect. Next, DOX-AuNP conjugates were subject to increasing temperatures, which enhanced DOX desorption from AuNP surface (Figure 3C). These results suggest desorption of DOX from AuNP surfaces is an endothermic process; conversely, adsorption is exothermic and spontaneous in nature, consistent with previous work on anthracene and benzene adsorption onto AuNP surfaces.⁴² All experimental results indicate DOX adsorption was not driven by electrostatic interaction, but rather by hydrophobic forces.

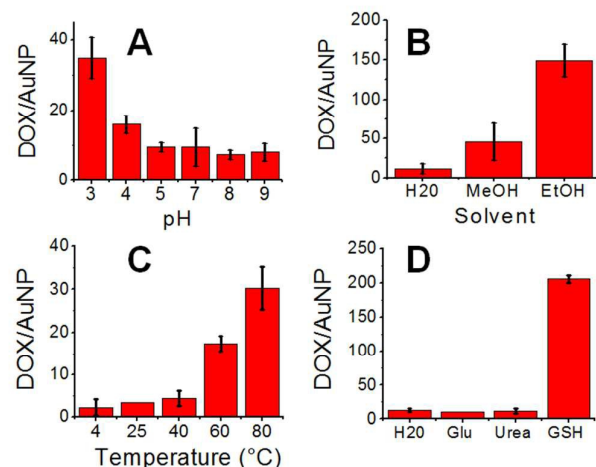
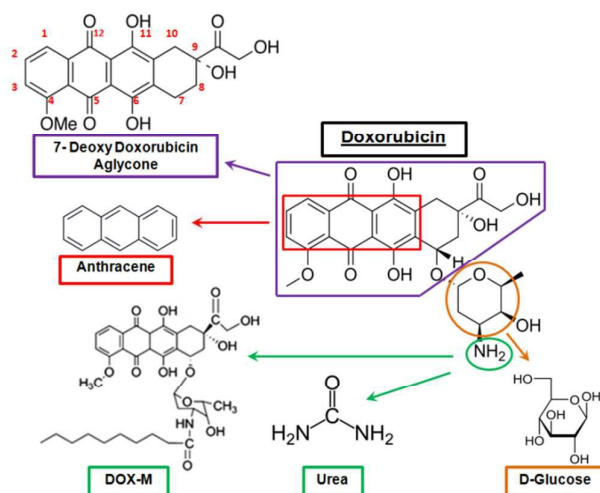


Figure 3. DOX desorption from AuNP in presence of varying pH (A), solvent (B) and thermal (C) conditions. (D) DOX desorption from AuNP upon addition of competitive molecules ([Glu], [Urea] = 45 mM, [GSH] = 182 μM).



Scheme 2. Chemical compounds used in this work mimicking potential DOX functional groups of interest in AuNP adsorption.

Identification of the molecular functionalities contributing to DOX-AuNP interaction.

To identify which DOX functional groups contribute to its adsorption, we studied the interaction between AuNP and compounds sharing structural similarities to DOX (Scheme 2). These analogs include anthracene (ANT), 7-deoxy doxorubicin aglycone (DDA), D-glucose (Glu), Urea, decanoic acid modified DOX (DOX-M) and glutathione (GSH), a thiolated compound, for comparison. The results showed that even high concentrations (45 mM, ~10,000 times DOX concentration) of glucose and urea were unable to displace DOX from AuNP surfaces (Figure 3D), while comparable levels (μM level) of anthracene could replace DOX (Figure 4A). Adsorption kinetics experiments further confirmed ANT, DDA, and DOX-M all adsorbed on AuNPs (Figure 4B) with even higher affinities for AuNP surfaces than possessed by DOX. This clearly demonstrates the amine group does not contribute to DOX-AuNP interactions, which is in agreement with the characterization of DOX-AuNP conjugates with X-ray photoelectron spectroscopy (XPS). As illustrated in Figure S8, N 1s and C 1s XPS spectra for DOX-AuNP clearly show binding energy peaks at 402.11, 400.08 eV (Figure S8A), and 285.40 eV (Figure S8B) in the de-convoluted peaks, attributable to the free amine and C-N groups of DOX, but not Au-N coordination, as it is well established that the binding energy of N 1s decreases by 1-3 eV upon binding to metallic surfaces due to a transfer of electron density from nitrogen to metals.^{43,44} Taken together, we reason that DOX adsorption onto AuNP surfaces is via the anthracene ring due to cation- π interactions with the adsorbed Au⁺ on AuNP surfaces, similar to previous studies on the adsorption of benzene and anthracene onto AuNP surfaces^{42,45}. MgCl₂ induced desorption (Figure S7B) further strengthened this hypothesis since Mg²⁺ ions may create cationic competition with Au⁺ for DOX. Although desorption is not highly pronounced, the

result is reasonable since it is the hydrophobic force rather than cation- π interaction that drives the DOXs to the AuNP surface. In addition, ethylenediaminetetraacetic acid (EDTA) was shown to inhibit DOX adsorption onto AuNPs (Figure S7C), presumably due to the coordination of Au⁺ ions by EDTA, leaving less Au⁺ available for DOX to interact with. The use of EDTA in this context comes with limitations related to charge repulsion. The negative charge associated with EDTA makes it difficult for the molecule to approach and coordinate with surface-bound Au⁺ due to repulsion from the negative citrate layer on AuNP. Nevertheless, the results of the MgCl₂ and EDTA experiments support the cation- π interaction theory. This hypothesis was further substantiated with modelling work.

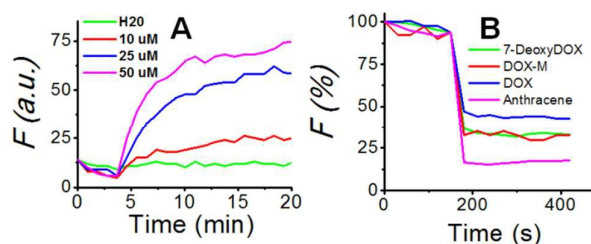


Figure 4. (A) Fluorescence intensity of DOX from DOX-AuNP conjugates upon addition of anthracene. (B) Fluorescence intensity of compounds structurally analogous or with relevant functional groups to DOX molecules upon addition of AuNP.

Modelling of the DOX-AuNP interaction

Theoretical models describing the interaction between AuNPs (assumed 0.5 nm in size to be relatively efficient with quantum mechanics modelling) and DOX were produced (Figure 5). The 0.5-nm AuNPs might underestimate the magnitude of the forces that govern the interaction between DOX and 13-nm AuNPs, but would not change the physiochemical nature of the interactions. DOX has 3 carbonyl groups in position 7, 9 and 10 (Figure 5a) which contribute to the stabilization of the molecular conformation through forming hydrogen bonds with nearby hydroxyl groups (e.g., at positions 9 and 42 as well as 10 and 43). The steric hindrance of C30 may favour hydrogen bonding between 7 and 44, or 7 and 40. Disruption of the proposed hydrogen bonds may increase the ionisation potential of DOX, facilitating DOX adsorption to AuNPs (Figure 6b). An earlier study reported DOX interactions with nanoscale particles is mainly due to van der Waals forces forming a S-conformation DOX layer on the particle surface (meaning the ring structures are directly interacting with the chitosan particle),⁴⁶ which is generally consistent with our isotherm data (Figure 1A). However, functional groups driving the absorption of DOX were not definitively identified, and may differ when interacting with

AuNPs from that with chitosan. To address these issues, we performed quantum molecular dynamics modelling to reveal the detailed mechanism of DOX-AuNP interaction (Figure S9).

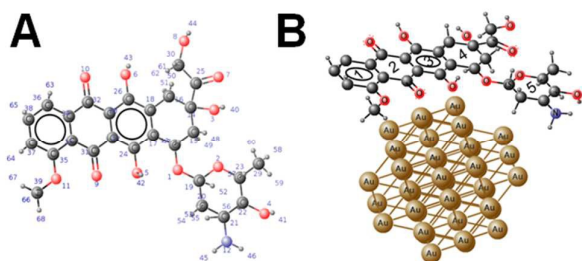


Figure 5. (A) Structure of Doxorubicin and (B) Doxorubicin with gold nanoparticles.

First, we calculated and compared the IR frequencies of DOX (with and without AuNPs) to explain the peak shift observed in FTIR spectra. Without AuNPs, the stretching vibrational frequency of the carbonyl group of DOX is temperature independent between 200 - 400 °K (Figure 6A-B). In the presence of AuNPs, the carbonyl stretch peak shifted to a higher frequency (Figure 6C). In addition to this up-field frequency shift, the peak of the carbonyl stretch splits due to the different carbonyl functionalities, in other words, the carbonyls on the ring and on the ketone may interact with AuNPs differently. Further, the intensity of the carbonyl stretch in ketones decreased drastically, indicating the carbonyl groups (positions 7, 9 and 10 in Figure 5a) are involved in DOX-AuNPs interactions. Similarly, the shift of frequency-fingerprint of the C=C of the anthracene ring ($\sim 1600\text{ cm}^{-1}$) demonstrates the involvement of the ring structure in the AuNP-DOX interaction (highlighted region in Figure 6). In contrast, the possibility of binding between the DOX amine group and AuNP via Au-N bonds is low, as evidenced by the low peak intensity of 386 cm^{-1} , the frequency of Au-N bond stretching.

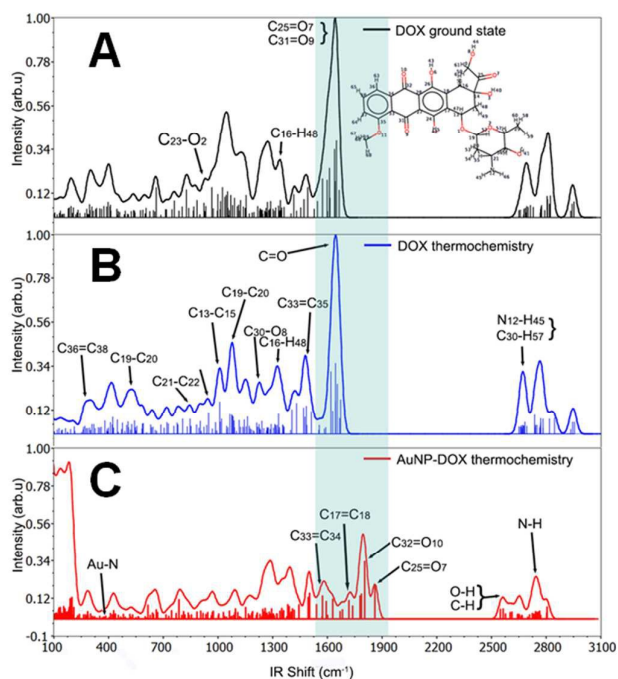


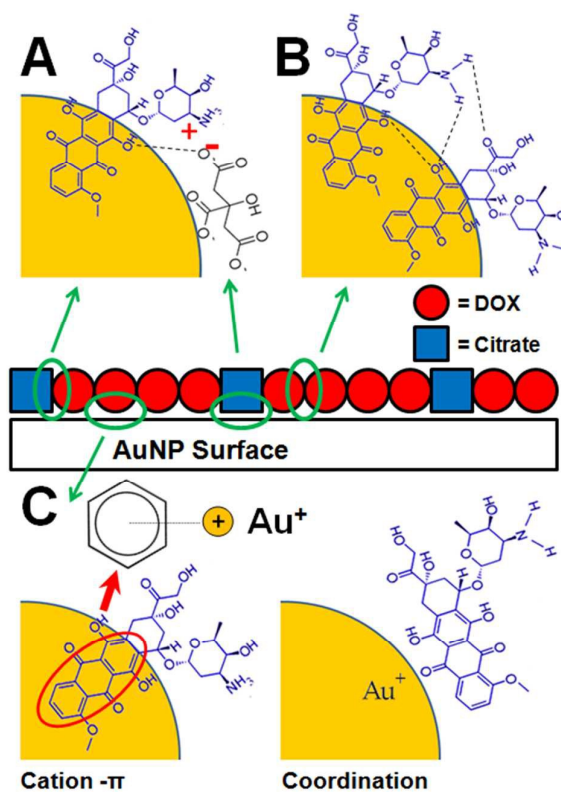
Figure 6. The IR spectrum showing the peak shifts in DOX in ground state at room temperature (A), excited state with increased temperature (B) and DOX-AuNP conjugates (C). Features are labelled in the Figure.

To further identify the contribution of each DOX functional group to its adsorption onto AuNP, molecular dynamics (MD) and quantum mechanics (QM) were employed to model the ground state conformations of the DOX-AuNP system. We constructed three models to differentiate the contribution of the amine group in the sugar ring from that of the anthracene ring. In model 1, we compared the binding of DOX molecules with that of their analogue lacking the amine group. The model demonstrated an 8.3% probability that ring 5 (the sugar ring containing the amine group) bends toward AuNP surfaces, potentially forming an Au-N bond. However, this bending phenomena was persistent with the DOX analog lacking the amine group in ring 5, suggesting the bending of DOX is not due to the formation of an Au-N bond, but likely attributable to π - σ attraction (where the σ bonds were from ring 5) that dominated the edge to face interaction.⁴⁷ In model 2, we evaluated the contribution from ring 5 and the carbonyl groups in ring 2 by applying a DOX analog lacking ring 5 to the AuNP (Figure S10A); the results demonstrated electrostatic interaction between the carbonyl of ring 2 and the AuNP surface. Next we modelled how AuNPs interact with anthracene, a DOX analog with only the rings 1-3 (model 3). In this model, DOX interacted with AuNPs by cation - π interactions (Figure S11) between the Au^+ cations adsorbed on the AuNP surface, and anthracene rings 1 and 3. The AuNP-anthracene interaction appeared with low frequencies ($< 400\text{ cm}^{-1}$) and involved the puckering of the ring

observed through the peak at $\sim 680\text{ cm}^{-1}$ (Figure S10B), where the =C-H bending appeared.

The DOX analog without ring 5 adsorbed on AuNP surface showed low carbonyl group stretching frequencies (Figure S10A), attributable to the direct anchoring of the two carbonyl groups (located on ring 2) to the AuNP surface. The carbonyl-Au coordination facilitates the cation- π interaction of rings 1 and 3 on the AuNP surface, synergistically contributing to the overall force of the DOX-AuNP interaction.

Combining the experimental work and theoretical modelling, we conclude the main forces that contribute to DOX adsorption onto AuNPs consist of π -cation interactions and Au-carbonyl coordination chemistry (Scheme 3C). Nevertheless, it is reasonable to expect contributions from intermolecular forces such as electrostatic attraction between DOX and residual citrate molecules (Scheme 3A) and hydrogen bonding between several DOX molecules (Scheme 3B). Considering the DOX adsorption with intermolecular interactions, the adsorbed DOX and a small number of residual citrate molecules form an assembled monolayer structure, impairing the charge-based stabilization of AuNPs due to decreased net surface charge relative to the original citrate-capped AuNPs.



Scheme 3. (A) Electrostatic interaction (+-) and hydrogen bonding (----) between adsorbed citrate and adsorbed DOX molecules on AuNP surfaces. (B) Hydrogen bonding between adsorbed DOX molecules on AuNP surface. (C) Cation- π and coordination chemistry between DOX and AuNP surface.

To examine the strength of the DOX-AuNP interaction, we evaluated DOX desorption in the presence of bovine serum albumin (BSA) and GSH, both of which are present in high concentration in blood and cytoplasm. BSA adsorbs on citrate-AuNPs through a mixed mechanism involving electrostatic, hydrophobic, and coordination chemistry while GSH adsorbs to AuNPs via thiol-gold bonds.^{48,49} Our results demonstrate GSH could displace DOX rapidly and efficiently ($\sim 70\%$ replacement over 60 min), demonstrating that the thiol-gold bond is stronger than the forces governing DOX-AuNPs interactions (Figure 7B, Figure 3D). BSA also facilitated DOX desorption, although not as efficiently as GSH with $\sim 18\%$ DOX desorbed in the presence of $\sim 0.7\text{ mM}$ BSA over 50 min (Figure 7A). Such DOX displacement by common blood-borne constituents are significant for *in vivo* drug delivery research, since the concentrations of GSH (μM level in blood and mM level in cytoplasm) and BSA ($\sim 0.7\text{ mM}$ in blood) used in this study were physiologically relevant.

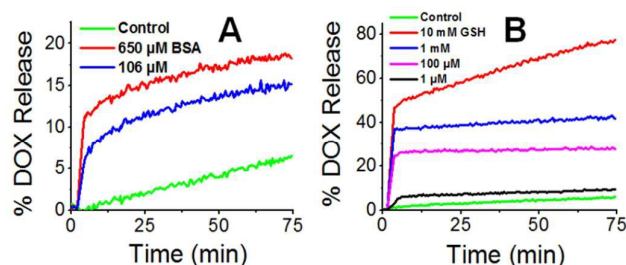


Figure 7. BSA (A) and GSH (B) induced DOX fluorescence signal increase via desorption from AuNP surface.

Conclusions

In summary, for the first time, we provide both empirical and theoretical evidence demonstrating the mechanism of DOX adsorption onto AuNP is based on cation- π interactions and formation of a DOX monolayer on the nanoparticle surface. DOX adsorption is proposed as a two-step process where hydrophobic forces first drive DOX molecules toward the AuNP surface prior to cation- π interactions and coordination chemistry between DOX and the cationic surface of AuNP anchoring DOX to AuNP surface and replacing most of the citrate molecules. Contrary to the conventional understanding, the contribution of the amine group in DOX to AuNP adsorption is negligible, though together with the hydrogen bonding as an intermolecular force, it may contribute to the formation of an adlayer on AuNP with residual citrate. Physiologically-relevant molecules (GSH and BSA) were shown to rapidly desorb DOX from the nanoparticle surface at physiological concentrations, an important point to consider for *in vivo* drug delivery and controlled release studies. Despite the simplicity of the DOX-AuNP interaction for drug loading, the nanoconjugate remains vulnerable to these physiological conditions. Stabilization methods such as co-adsorption of DNA or PEG should be considered when employing simple DOX-AuNP chemistry. Considering the volume of research articles dedicated to DOX-AuNP delivery systems, detailed knowledge of the nature of this fundamental interaction may allow researchers to better design delivery systems and estimate therapeutic drug loading and release parameters, therefore increasing anticancer drug efficiencies both *in vivo* and *in vitro*.

Experimental details

Materials and Methods

Chemicals Doxorubicin hydrochloride, glutathione, bovine serum albumin and the citrate assay kit were purchased from Sigma-Aldrich (St. Louis, MO). Polystyrene 96-well plates were purchased from Corning Inc. (NY) and microcentrifuge tubes (cat. no. 02-681-284), ethanol, methanol, and NaCl were purchased

from Fisher Scientific (Ottawa, ON, Canada). KBr spectrograde powder was purchased from International Crystal Labs (Garfield, NJ). HEPES salt and trisodium citrate were purchased from Alfa Aesar (Parkridge Rd Ward Hill, MA). 7-Deoxy Doxorubicin Aglycone was purchased from Toronto Research Chemicals Inc. and Anthracene was supplied by J.T.Baker chemicals. DOX-M was synthesized following reported protocols and confirmed with NMR and Mass spectrometry.⁵⁰ AuNPs were synthesized via the well-established citrate reduction method.⁵¹ Nanopure 18.2M Ω cm water was used in all experimentation.

DOX Quantification Un-adsorbed or “free” doxorubicin was quantified by fluorescence measurement in all experimentation using excitation/emission wavelengths of 480/580 nm. These “free” values were subsequently converted to molar concentrations using calibration curves for doxorubicin to determine the number of loaded or desorbed drug molecules per AuNP. Fluorescent measurements were carried out in 96-well plates. For quantitative studies, polyethylene glycol was included in the plate well buffer to inhibit non-specific sorptive loss of DOX as recently reported on by our group.⁵² In all experimentation, doxorubicin fluorescence (excitation/emission: 480/580 nm) and AuNP UV-Vis absorbance was quantified using a TECAN infinite M10000 PRO micro-plate reader.

Adsorption Kinetics and AuNP aggregation In order to study the kinetics of DOX adsorption onto the nanoparticle surface, fluorescence of a DOX sample (90 μ L) was measured for six minutes before the addition of AuNP (10 μ L, \sim 10 nM or \sim 30 nM). To study the effect of DOX on AuNP aggregation, DOX solutions of various concentrations were added to wells containing a constant volume of AuNP (10 nM) before recording the absorbance spectra.

DOX Adsorption Isotherm For all adsorption studies, equal volumes of DOX solution (dissolved in nanopure H₂O with different concentrations) and gold nanoparticles were used to ensure uniform surface coverage.⁴⁰ Typically, the DOX and AuNP solutions were mixed in 1.5 mL microcentrifuge tubes and centrifuged at 12,700 rpm for 4 minutes to form DOX-AuNP conjugate precipitates. Thereafter, 20 μ L of the supernatant solution (containing “free” DOX) was carefully transferred to plate wells each containing 80 μ L of HEPES-PEG 20K buffer solution (final PEG 20K concentration: \sim 50 mM, final HEPES concentration: 4-80 mM, where 80 mM HEPES buffer was used to maintain the sample pH to avoid pH dependent fluorescence variation). To test the effect of pH on adsorption, 3 μ L of pH citrate buffer (0.3 M, various pH values) was added to DOX solutions prior to mixing with the AuNP solution. To evaluate the effect of salt on adsorption, NaCl (up to 5 μ L) was added to the DOX solution prior to mixing with the AuNP solution. In these studies, AuNPs were first rinsed with Nanopure water to

remove residual salt during AuNP synthesis. This step helped to prevent AuNP aggregation due to solvent-salt synergistic effects.⁵³ For EDTA effect on DOX adsorption, EDTA (2 μ L, 100 μ M) was added to AuNP (25 μ L, 13 nM) prior to the addition of DOX (25 μ L, 4 μ M). Adsorbed DOX was calculated using DOX fluorescence in the supernatant. The calibration was performed using freshly prepared DOX standard solutions with the HEPES-PEG buffer.

Adsorption of DOX Analogs To study the adsorption kinetics of DOX analogs onto AuNPs, fluorescence kinetic measurements were conducted. Briefly, 88 μ L of HEPES buffer (5 mM, pH 7.6) was added to a 96-well plate followed by 2 μ L of stock analog solution in EtOH. Fluorescence measurements were recorded every 30 sec, and after 150 sec, 10 μ L of AuNP (10 nM) was added and gently mixed into the wells using a pipette. Nanopure water rather than AuNP was added to the control wells. All data were normalized to 100% fluorescence representing the initial fluorescence intensity measured in each well prior to the addition of AuNP. Fluorescence spectra were measured using the following excitation/emission wavelengths (nm): DOX: 480/580, DOX-M: 490/586, DeoxyDOX: 490/576, Anthracene: 252/376.

Desorption Studies To evaluate the effects of pH, temperature, salt, and solvent concentrations on DOX desorption, drug-nanoparticle conjugates were prepared in equal volumes (as mentioned previously). In desorption studies, a drug-to-nanoparticle concentration ratio of \sim 300:1 was used to ensure \sim 100% adsorption of DOX onto AuNP (as evidenced by the near total quenching of DOX at this ratio). After mixing AuNP and DOX (both prepared in nanopure water without buffer) in 1.5 mL tubes, the conjugate samples were treated with pH buffer (2 μ L, 0.35 M, various pH values), solvent (ethanol, methanol, 25 μ L), or temperature (15 min exposure). For the temperature effect studies, high temperature samples were submerged in a water bath with water temperature monitored using a thermocouple. Samples treated at 4°C and 25°C were achieved by keeping conjugate solutions in a refrigerator (4°C) or bench top (room temperature: \sim 25°C) for 15 min, respectively. For MgCl₂-ethanol desorption studies, AuNP were rinsed prior to treatment to decrease previously mentioned solvent-salt synergistic effects. Conjugate samples were again centrifuged at 12,700 RPM to form AuNP precipitates and resultant supernatant samples were analyzed for DOX concentration as outlined above. To study the displacement of DOX from AuNPs by anthracene, increasing concentrations of aqueous anthracene solutions were added to wells containing DOX-AuNP conjugates with equivalent volumes of Nanopure water used in control groups. DOX-AuNP conjugate fluorescence measurements were taken for several min prior to the addition of anthracene. For both GSH and BSA-induced DOX desorption

studies, DOX and AuNP were mixed in 96-well plates prior to fluorescence measurements. Different concentrations of GSH and BSA solutions were then added to plate wells and mixed by pipetting before subsequent fluorescent measurements at excitation/emission: 480/580 nm.

Citrate Assay DOX-AuNP conjugate mixtures (1153:1 drug-to-nanoparticle molar concentration ratio) and AuNP controls were prepared as outlined above. The mixtures were centrifuged and the citrate concentration in the resulting supernatant solution was quantified using a citrate assay kit as per manufacturer's directions (Sigma Aldrich, Catalog Number: MAK057). Following an enzymatic reaction, the concentration of free citrate in solution correlated to the production of a fluorescent marker dye. The resultant citrate concentrations in the supernatant solutions were calculated by comparing the sample fluorescence to fluorescence values obtained from known citrate standard solutions provided in the kit.

Infrared Spectroscopy Fourier Transform Infrared Absorption Spectra were obtained by a Thermo Nicolet 6700 FT-IR Spectrometer. DOX-AuNP conjugate mixtures (1538:1 concentration ratio) and AuNP mixtures were prepared in microcentrifuge tubes ($n=12$). Following repeated centrifugation and rinsing steps, precipitate solutions were combined and allowed to dry in light-protected weigh boats for 48 h. Subsequently, 150 mg of KBr was added to each of the samples before being pressed into round pellets and dehydrated. The samples were analyzed using the infrared spectrometer (samples measured against KBr, 256 scans per sample, 4 cm⁻¹ resolution). Spectra baselines were corrected using OMNIC software.

X-Ray Photoelectron Spectroscopy Silicon substrates were sonicated in acetone for 10 minutes prior to drying. For AuNP samples, AuNP were concentrated via centrifugation and directly dropped onto the surface of the silicon substrate. For DOX-AuNP sample, AuNP were mixed with aqueous DOX and concentrated via centrifugation. To maximize the amount of sample recovered, DOX-AuNP conjugates were briefly sonicated to remove adsorbed conjugates from the microcentrifuge tube surface before being directly dropped onto the silicon substrate. Prior to analysis, samples were allowed to dry in a fume hood overnight. XPS analyses were performed using a Thermo-VG Scientific ESCALab 250 Microprobe equipped with a monochromatic Al Ka X-Ray source (1486.6 eV). All spectra were processed and analyzed using CasaXPS software.

Transmission electron microscopy TEM micrographs were obtained using a Phillips CM30 microscope operated with an accelerating voltage of 250 kV. As-prepared AuNP and DOX-

AuNP conjugate solutions were dropped onto lacey carbon-coated TEM grids and imaged at various magnifications.

Theoretical investigations To thoroughly understand interactions between DOX and AuNP observed empirically, we modelled molecular dynamics (MD) varying influences of functional groups under experimental conditions. The DOX pdb file was obtained from the Drug Data Bank and the hydrogens were added using MarvinSketch software (version 15.6.29.0, 2015, ChemAxon (<http://www.chemaxon.com>)). The AuNP pdb file was made with OpenMD nanoparticle builder with forcefield SuttonChen along the lattice constant of gold, 4.08 Å. The AuNP pdb and DOX pdb were imported into MarvinSketch and merged into one system. The modelling was made using MOPAC2012 at PM7 level of theory.⁵⁴ The visualisation and analysis of quantum calculations were made using Gabedit.⁵⁵ The obtained geometry optimisation output file was used for 10 ns molecular dynamic (MD) modelling of the ground state geometry with universal forcefield (UFF).⁵⁶ MarvinSketch_{__}was used for drawing, displaying and characterizing chemical structures, substructures and reactions.

Acknowledgements

This work was financially supported by Canadian Institutes of Health Research (CIHR), the Nova Scotia Health Research Foundation (NSHRF), the Sydney Tar Ponds Agency, as well as Public Works and Government Services of Canada (formerly part of ECBC) through grants supporting the Industrial Research Chairs and ACENet undergraduate Fellowship. Dennis Curry is supported by a CIHR-CGS research award as well as a trainee award from the Beatrice Hunter Cancer Research Institute with funds provided by the Breast Cancer Society of Canada/QEII Foundation/BHCRHI Traineeship for Breast Cancer Research as part of the Cancer Research Training Program. The authors would like to thank Dr. Dale Keefe of Cape Breton University for access to FTIR instrumentation as well as Dr. Feng Wang and Biwu Liu of the University of Waterloo for inspiring discussions and assistance with AuNP synthesis. All computational work was completed using ACENet and other Compute Canada cluster and facilities.

Supporting Information Available: DOX-AuNP absorption spectra and colored solution images, citrate displacement data, original DOX-AuNP loading isotherm, XPS data and TEM micrographs, modelling data. This material is available free of charge via the Internet at XXX

References

1. I. Judson, J. Verweij, H. Gelderblom, J. T. Hartmann, P. Schöffski, J.-Y. Blay, J. M. Kerst, J. Sufliarsky, J. Whelan, P. Hohenberger, A. Krarup-Hansen, T. Alcindor, S. Marreaud, S. Litière, C. Hermans, C. Fisher, P. C. W. Hogendoorn, A. P. dei Tos and W. T. A. van der Graaf, *The Lancet Oncology*, 15, 415-423.
2. M. M. Gottesman, T. Fojo and S. E. Bates, *Nat Rev Cancer*, 2002, 2, 48-58.
3. P. J. Hesketh and P. Sanz-Altamira, *Supportive care in cancer : official journal of the Multinational Association of Supportive Care in Cancer*, 2012, 20, 653-656.
4. J. E. Anderson, J. M. Hunt and I. E. Smith, *British Medical Journal (Clinical research ed.)*, 1981, 282, 423-424.
5. K. Chatterjee, J. Zhang, N. Honbo and J. S. Karliner, *Cardiology*, 2010, 115, 155-162.
6. T. M. Allen and F. J. Martin, *Seminars in oncology*, 2004, 31, 5-15.
7. A. Gabizon, H. Shmeeda and Y. Barenholz, *Clin Pharmacokinet*, 2003, 42, 419-436.
8. A. Gabizon, R. Catane, B. Uziely, B. Kaufman, T. Safra, R. Cohen, F. Martin, A. Huang and Y. Barenholz, *Cancer research*, 1994, 54, 987-992.
9. D. Kim, Y. Y. Jeong and S. Jon, *ACS nano*, 2010, 4, 3689-3696.
10. V. Bagalkot, O. C. Farokhzad, R. Langer and S. Jon, *Angewandte Chemie (International ed. in English)*, 2006, 45, 8149-8152.
11. S. R. Jean, D. V. Tulumello, C. Riganti, S. U. Liyanage, A. D. Schimmer and S. O. Kelley, *ACS Chemical Biology*, 2015, DOI: 10.1021/acschembio.5b00268.
12. P. Ghosh, G. Han, M. De, C. K. Kim and V. M. Rotello, *Advanced Drug Delivery Reviews*, 2008, 60, 1307-1315.
13. G. F. Paciotti, D. G. I. Kingston and L. Tamarkin, *Drug Development Research*, 2006, 67, 47-54.
14. Y. Cheng, A. C. Samia, J. D. Meyers, I. Panagopoulos, B. Fei and C. Burda, *Journal of the American Chemical Society*, 2008, 130, 10643-10647.
15. P. S. Ghosh, C.-K. Kim, G. Han, N. S. Forbes and V. M. Rotello, *ACS nano*, 2008, 2, 2213-2218.
16. X.-Q. Zhang, X. Xu, R. Lam, D. Giljohann, D. Ho and C. A. Mirkin, *ACS nano*, 2011, 5, 6962-6970.
17. C. T. Zhao and Z. B. Liu, *Zhongguo yi xue ke xue yuan xue bao. Acta Academiae Medicinae Sinicae*, 2014, 36, 324-329.

ARTICLE

Journal Name

18. K. Saha, S. S. Agasti, C. Kim, X. Li and V. M. Rotello, *Chemical Reviews*, 2012, 112, 2739-2779.
19. R. Shukla, V. Bansal, M. Chaudhary, A. Basu, R. Bhonde and M. Sastry, *Langmuir*, 2005, 21, 10644 - 10654.
20. R. Arvizo, R. Bhattacharya and P. Mukherjee, *Expert opinion on drug delivery*, 2010, 7, 753-763.
21. H. Jans and Q. Huo, *Chemical Society Reviews*, 2012, 41, 2849-2866.
22. H. Park, J. Yang, J. Lee, S. Haam, I.-H. Choi and K.-H. Yoo, *ACS nano*, 2009, 3, 2919-2926.
23. S. K. Libutti, G. F. Paciotti, A. A. Byrnes, H. R. Alexander, Jr., W. E. Gannon, M. Walker, G. D. Seidel, N. Yuldasheva and L. Tamarkin, *Clinical cancer research : an official journal of the American Association for Cancer Research*, 2010, 16, 6139-6149.
24. F. Wang, Y.-C. Wang, S. Dou, M.-H. Xiong, T.-M. Sun and J. Wang, *ACS nano*, 2011, 5, 3679-3692.
25. X. Huang and M. A. El-Sayed, *Journal of Advanced Research*, 2010, 1, 13-28.
26. W. Lu, C. Xiong, G. Zhang, Q. Huang, R. Zhang, J. Z. Zhang and C. Li, *Clinical cancer research : an official journal of the American Association for Cancer Research*, 2009, 15, 876-886.
27. J. You, G. Zhang and C. Li, *ACS nano*, 2010, 4, 1033 - 1041.
28. F. Kong, X. Zhang, H. Zhang, X. Qu, D. Chen, M. Servos, E. Mäkilä, J. Salonen, H. A. Santos, M. Hai and D. A. Weitz, *Advanced Functional Materials*, 2015, 25, 3330-3340.
29. S. Aryal, J. J. Grailer, S. Pilla, D. A. Steeber and S. Gong, *Journal of Materials Chemistry*, 2009, 19, 7879-7884.
30. M. Prabakaran, J. J. Grailer, S. Pilla, D. A. Steeber and S. Gong, *Biomaterials*, 2009, 30, 6065-6075.
31. N. S. Elbially, M. M. Fathy and W. M. Khalil, *Physica Medica*, 2014, 30, 843-848.
32. A. Z. Mirza and H. Shamshad, *European journal of medicinal chemistry*, 2011, 46, 1857-1860.
33. X. Zhang, M. R. Servos and J. Liu, *Langmuir*, 2012, 28, 3896-3902.
34. T. Doane and C. Burda, *Advanced drug delivery reviews*, 2013, 65, 607-621.
35. J.-W. Park and J. S. Shumaker-Parry, *ACS nano*, 2015, 9, 1665-1682.
36. J.-W. Park and J. S. Shumaker-Parry, *Journal of the American Chemical Society*, 2014, 136, 1907-1921.
37. K. C. Barick, S. Nigam and D. Bahadur, *Journal of Materials Chemistry*, 2010, 20, 6446-6452.
38. X. Zhang, M. R. Servos and J. Liu, *Journal of the American Chemical Society*, 2012, 134, 7266-7269.
39. X. Zhang, B. Liu, N. Dave, M. R. Servos and J. Liu, *Langmuir*, 2012, 28, 17053-17060.
40. B. L. Darby and E. C. Le Ru, *Journal of the American Chemical Society*, 2014, 136, 10965-10973.
41. Z. Liu, X. Sun, N. Nakayama-Ratchford and H. Dai, *ACS nano*, 2007, 1, 50-56.
42. A. Kumar, S. Mandal, S. P. Mathew, P. R. Selvakannan, A. B. Mandale, R. V. Chaudhari and M. Sastry, *Langmuir*, 2002, 18, 6478-6483.
43. Z. Li, H. Chen, H. Bao and M. Gao, *Chemistry of Materials*, 2004, 16, 1391-1393.
44. S. Mondal, U. Rana and S. Malik, *Chemical Communications*, 2015, DOI: 10.1039/C5CC03981A.
45. M. Pagliai, S. Caporali, M. Muniz-Miranda, G. Pratesi and V. Schettino, *The Journal of Physical Chemistry Letters*, 2012, 3, 242-245.
46. P. Shan, J.-W. Shen, D.-H. Xu, L.-Y. Shi, J. Gao, Y.-W. Lan, Q. Wang and X.-H. Wei, *RSC Advances*, 2014, 4, 23730-23739.
47. C. A. Hunter and J. K. M. Sanders, *Journal of the American Chemical Society*, 1990, 112, 5525-5534.
48. S. H. Brewer, W. R. Glomm, M. C. Johnson, M. K. Knag and S. Franzen, *Langmuir*, 2005, 21, 9303-9307.
49. J. Gao, X. Huang, H. Liu, F. Zan and J. Ren, *Langmuir*, 2012, 28, 4464-4471.
50. C. H. Liang, W. L. Ye, C. L. Zhu, R. Na, Y. Cheng, H. Cui, D. Z. Liu, Z. F. Yang and S. Y. Zhou, *Mol Pharm*, 2014, 11, 1378-1390.
51. G. Frens, *Nature*, 1973, 241, 20-22.
52. D. Curry, H. Scheller, M. Lu, M. Mkandawire, M. R. Servos, S. Cui, X. Zhang and K. D. Oakes, *RSC Advances*, 2015, 5, 25693-25698.
53. X. Han, J. Goebel, Z. Lu and Y. Yin, *Langmuir*, 2011, 27, 5282-5289.
54. J. D. C. Maia, G. A. Urquiza Carvalho, C. P. Manguiera, S. R. Santana, L. A. F. Cabral and G. B. Rocha, *Journal of Chemical Theory and Computation*, 2012, 8, 3072-3081.

Journal Name

ARTICLE

55. A.-R. Allouche, *Journal of Computational Chemistry*, 2011, 32, 174-182. *American Chemical Society*, 1992, 114, 10024-10035.
56. A. K. Rappe, C. J. Casewit, K. S. Colwell, W. A. Goddard and W. M. Skiff, *Journal of the*